Available online at www.sciencedirect.com
ScienceDirect
Journal of Magnetic Resonance 190 (2008) 105–112
JMR Journal of Magnetic Resonance
www.elsevier.com/locate/jmr

Monitoring redox-sensitive paramagnetic contrast agent by EPRI, OMRI and MRI

Fuminori Hyodo [a], Ramachandran Murugesan [a,1], Ken-ichiro Matsumoto [a,b], Emi Hyodo [a], Sankaran Subramanian [a], James B. Mitchell [a], Murali C. Krishna [a,*]

[a] *Radiation Biology Branch, Center for Cancer Research, National Cancer Institute, Building 10, Room B3B69, NIH, Bethesda, MD 20892-1002, USA*
[b] *Heavy-Ion Radiobiology Research Group, National Institute of Radiological Science, Chiba, Japan*

Received 8 May 2007; revised 16 October 2007
Available online 30 October 2007

Abstract

A comparative study of tissue redox-status imaging using commonly used redox sensitive nitroxides has been carried out using electron paramagnetic resonance imaging (EPRI), Overhauser magnetic resonance imaging (OMRI) and conventional T_1-weighted magnetic resonance imaging, MRI. Imaging studies using phantoms of different nitroxides at different concentration levels showed that EPRI and OMRI sensitivities were found to be linearly dependent on line width of nitroxides up to 2 mM, and the enhancement in MRI intensity was linear up to 5 mM. The sensitivity and resolution of EPRI and OMRI images depended significantly on the line width of the nitroxides whereas the MRI images were almost independent of EPR line width.

Reduction of the paramagnetic 3-carbamoyl-2,2,5,5-tetramethylpyrrolidine-1-oxyl (3CP) by ascorbic acid (AsA) to the diamagnetic by hydroxylamine was monitored from a sequence of temporal images, acquired using the three imaging modalities. The decay rates determined by all the three modalities were found to be similar. However the results suggest that T_1-weighted MRI can monitor the redox status, in addition to providing detailed anatomical structure in a short time. Therefore, a combination of MRI with nitroxides as metabolically responsive contrast agents can be a useful technique for the in vivo imaging probing tissue redox status.
Published by Elsevier Inc.

Keywords: Redox sensitive contrast agent; EPRI; MRI; OMRI; Nitroxide

1. Introduction

A variety of intracellular molecules such as GSH, thioredoxins, NADPH, flavins, ascorbic acid (AsA), etc. contribute to the overall redox status in tissues [1]. Collectively, the reducing species determine the redox status of tumor, and are likely to influence the response of a particular tissue to oxidative stress. It is widely believed that tumor redox status is an important parameter that may be related to tumor growth and therapy [2,3]. Hence it is of interest to develop non-invasive imaging methods to determine the in vivo redox status. In this direction, in vivo EPRI is emerging as a viable redox status imaging modality. Spatially resolved redox data, obtained using EPRI technique have shown that tumors are highly reducing and hypoxic compared to normal tissues [3,4]. These EPRI measurements are based on the fact that the paramagnetic nitroxides are reduced to the corresponding diamagneticone-electron reduction product (Fig. 1A), hydroxylamine in cellular incubations as well as in vivo [5–8]. It was postulated that nitroxides can accept cellular reducing equivalents, especially from the mitochondrial electron transport chain that would have otherwise gone to the reduction of molecular oxygen [9]. Hence, spatially resolved pharmacokinetics of nitroxides in an EPR experiment can report on differences that exist in various tissues which may display different redox status.

* Corresponding author. Fax: +1 301 480 2238.
E-mail address: murali@helix.nih.gov (M.C. Krishna).
[1] Permanent Address: School of Chemistry, Madurai Kamaraj University, Madurai, India.

1090-7807/$ - see front matter Published by Elsevier Inc.
doi:10.1016/j.jmr.2007.10.013

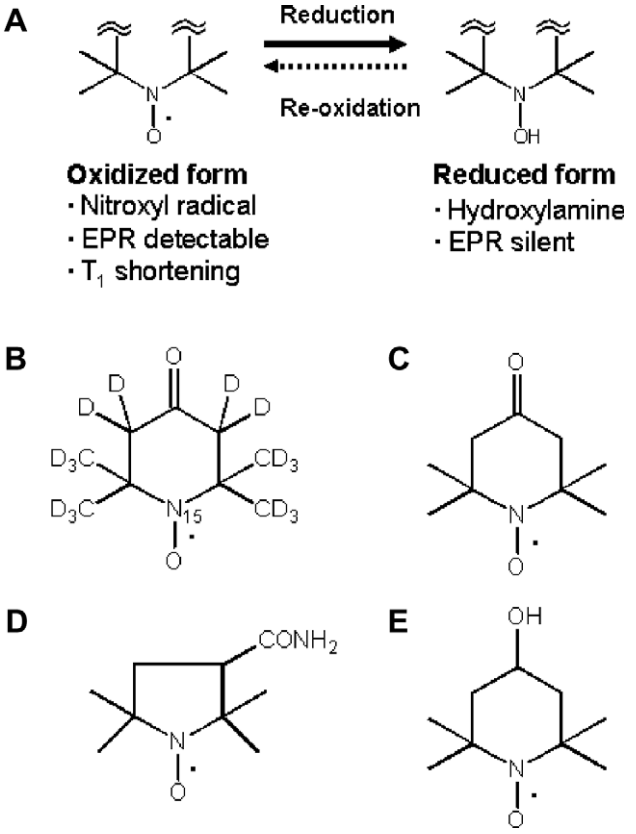

Fig. 1. (A) Reversible one-electron reduction/oxidation showing the interconversion and the molecular structure of the four nitroxides, (B) ^{15}N-PDT, (C) Tempone, (D) 3CP and (E) Tempol used in this work.

EPRI using nitroxides as a tracer was first demonstrated by Berliner and Fuji [10] and its pharmacokinetics monitored in tumor bearing animals in a subsequent paper [11]. Though EPRI is developing as an emerging imaging modality, it does not provide well-resolved morphological information, requiring the use of fiducials for a proper region of interest identification [12,13]. Overhauser MRI (OMRI) is a double resonance technique and couples the advantages of MRI for spatial resolution with the sensitivity of EPR by making use of the Overhauser effect [14–16]. It has the potential of adding this missing anatomical information to the functional, redox or pO_2 images [17]. The Overhauser enhancement depends on the line width of the paramagnetic agent, which in turn depends on oxygen concentration [18], making it possible for co-registration of the anatomical structure with the corresponding oxygen status. Using OMRI and utilizing the differences in hyperfine patterns (both position and multiplicity) it has been possible to use the infusion of isotopically differently (^{15}N and ^{14}N) substituted nitroxides to investigate extra- and intracellular redox status simultaneously [19].

Though the use of nitroxide as a T_1-enhancing MRI contrast agent was realized early [20–23], the bio-reduction and rapid clearance have made them less useful than the metal-based Gd^{3+} complex contrast agents [24,25], which had a long biological half life and high molar relaxivity, compared with the single, odd-electron containing nitroxides. However, the bio-reduction of nitroxides can be monitored to effectively probe the redox status of tissues [4,26]. Therefore, nitroxides can play a unique dual role both as contrast agent and as redox-status reporters, with the availability of MR scanners in recent times with efficient pulse sequences such as spoiled gradient echo (SPGR) method for rapid imaging. Our study revealed that, coupled with the advantages of fast multi-slice measurement and high quality anatomical information, nitroxides as redox sensitive contrast in MRI can provide, indirectly via T_1 contrast, the bio-reduction rates, and hence report on tissue redox status.

Currently three different techniques, viz, EPRI, OMRI and MRI are available for redox imaging using nitroxides. Each one of them has its own capabilities and limitations. Based on the requirement of specific application, one modality may be preferred over the other. To make an appropriate selection, it would be of interest to make a comparative assessment of the performance of each of them in monitoring the redox status. This study makes such an attempt by using four nitroxides, (^{15}N-PDT, Tempone, 3CP and Tempol, whose structures are shown in Fig. 1B–E, and expanded names given below under materials and methods) and evaluating the relative advantages of EPRI, OMRI and MRI.

2. Materials and methods

2.1. Chemical

^{15}N-PDT (4-oxo-2,2,6,6-tetramethyl piperidine-d_{16}-1-^{15}N-oxyl) was purchased from CDN Isotopes inc (Quebec, Canada). Other nitroxides, Tempone (4-oxo-2,2,6,6- tetramethyl-1-piperidynyloxyl), 3CP (3-carbamoyl-2,2,5,5-tetramethylpyrrolidine-*N*-oxyl) and Tempol (4-hydroxy-2,2,6,6,-tetramethyl-1-piperidynyloxyl) (see Fig. 1B–D) were purchased from Sigma–Aldrich Chem. Co. (St. Louis, MO). Gd-DTPA (Magnevist) was purchased from BerLex laboratories (Wayne, Germany). Distilled, deionized water was used for all experiments. The other materials used were of analytical grade.

2.2. EPR spectroscopy and imaging

A seven-tube phantom, each tube (4.7 mm i.d.) containing 0, 0.25, 0.50, 0.75, 1.0, 1.5, 2.0 mM aqueous solutions of the nitroxide contrast agents, as shown in Fig. 2A, was used for performance evaluation. EPR spectra were obtained by an X-band spectrometer, and 2D spatial images perpendicular to the axes of the tubes using a 300 MHz CW EPR Imaging spectrometer [27]. These images are given in Fig. 2 (left column), and the concentration-dependence of the image intensity and SNR are plotted in Fig. 3A (top row). The spectrometer bridge was based on a standard hybrid T configuration with automatic

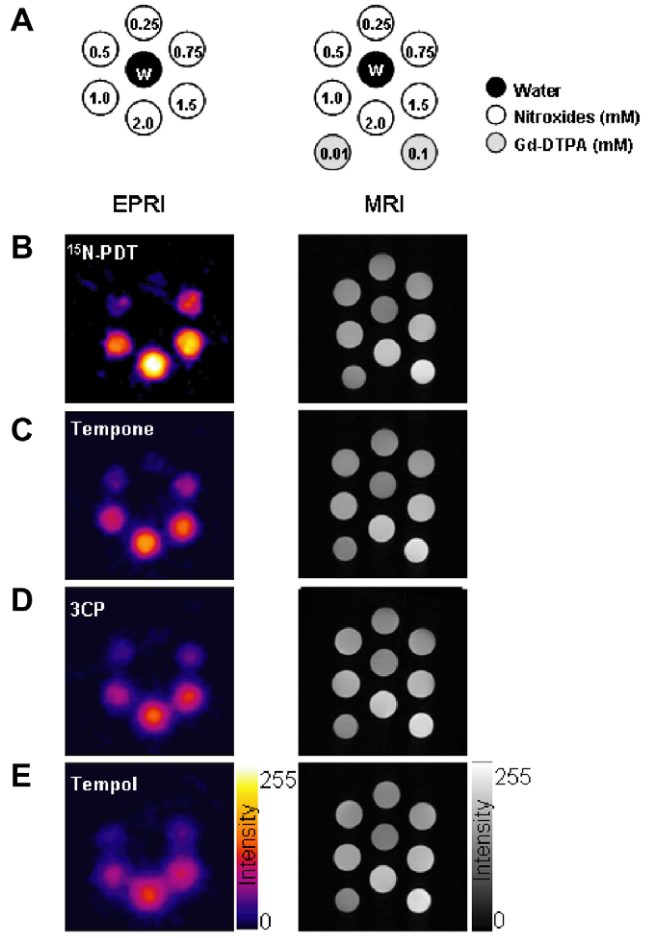

Fig. 2. The phantom images of four nitroxides obtained by EPRI and MRI. (A) Schematics of the phantom. Additionally two tubes of 0.01 and 0.1 mM Gd-DTPA solution were added during MRI measurement. The EPRI (Left column) and MR (right column) intensity images of (B) ^{15}N-PDT, (C) Tempone, (D) 3CP, (E) Tempol were described. *EPRI* conditions were follows; 18 projections were obtained every 1 min. FOV was 3.2 × 3.2 cm. Radio frequency was 300 MHz, radio frequency power 2.5 mW, field modulation frequency was 13.5 kHz, time constant 0.01 s, gradient was 4.7 G/cm, sweep width was 50 G. *MRI:* SPGE sequence (TR = 75 ms, TE = 3 ms, Flip angle = 45°, NEX = 2) was employed to observe T_1 effect. Pixel resolution was 256 × 256. FOV was 3.2 × 3.2 cm. All measurements were performed at room temperature (25 ± 2 °C).

frequency control capability. Signal detection was carried out by sinusoidal modulation and subsequent phase-sensitive detection. A parallel coil resonator (25 mm diameter and 25 mm length) was used for all experiments. EPR measurement conditions were as follows:

2.2.1. X-band EPR

Microwave power, 1 mW; field modulation frequency, 100 kHz; field modulation amplitude 0.05 G for both ^{15}N-PDT and Tempone; 0.24 G for 3CP; 0.38 G for Tempol; time constant, 0.003 s; sweep width, 0.5–2 G.

2.2.2. 300 MHz EPR

Radio frequency (RF) power, 2.5 mW; field modulation frequency, 13.5 kHz; modulation amplitude 0.3 G for both ^{15}N-PDT and Tempone; 0.7 G for 3CP; 1.2 G for Tempol; time constant, 0.01 s; sweep width, 10 G; scan time, 54 s; field gradient, 4.7 G/cm; and number of averages, 4. EPR image was reconstructed as a 128 × 128 matrix by filtered back-projection method using Shepp-Logan filter. FOV was 3.2 cm × 3.2 cm.

2.3. OMRI

A similar seven-tube phantom (4.7 mm i.d.) containing 0, 0.2, 0.5, 1, 2, 5, 10 mM ^{15}N-PDT, 3CP and Tempol solutions (Fig. 4A) was used for OMRI experiments. OMRI imaging was performed using standard spin warp gradient echo sequence where each phase encoding step was preceded by an EPR saturation pulse to elicit the Overhauser enhancement [17]. All OMRI studies employed the following conditions: TR, 1200 ms; TE, 25 ms; TEPR, 600 ms; number of phase-encoding gradient steps, 64; NEX, 4; FOV, 3.2 cm × 3.2 cm; slice thickness, 30 mm; scanning time, 60 s; Details of the scanner are presented elsewhere [17].

2.4. MRI

For MRI measurements, two other tubes (3.5 mm i.d.), containing 0.01 and 0.1 mM aqueous solutions of Gd^{3+}-DTPA as a standard marker were additionally incorporated into the phantom (Fig. 2A). To compare with OMRI, the tubes were prepared as described in OMRI methods and two additional high concentration tubes (15, 20 mM) were added. MRI measurements were performed at 4.7 T controlled with ParaVision® 3.0.1 (Bruker BioSpin MRI GmbH, Rheinstetten, Germany) at room temperature (25 ± 2 °C). To perform T_1 mapping, spin echo images were obtained using a multi-slice multi-echo (MSME) sequence with 5 different repetition times (TR: 4800, 3200, 1600, 800 and 400 ms). The scan time for T_1 mapping image sets (NEX = 2) by the MSME sequence was 46 min. SPGR (also referred to as gradient echo fast imaging, GEFI) (TR = 75 ms, TE = 3 ms, Flip angle = 45°, NEX = 16) was employed to observe the T_1 effect. The scan time for an image set (which included 2 slices) by the SPGR sequence was 160 s. Other typical parameters were as follows: image dimension, 256 × 256; FOV, 3.2 cm × 3.2 cm; slice thickness, 2.0 mm and number of slices, 2.

2.5. Redox imaging

The reduction of 3CP by AsA was used to demonstrate the redox imaging capability by the three techniques. The schematics of the four tube phantoms are shown in Fig. 5A. Tube 1 contained PBS in the absence of 3CP. Tube 2 and 3 contained 2 mM 3CP with 5 and 10 mM AsA/phosphate buffered saline (PBS, pH 7.4), respectively. Tube 4 was filled with 2 mM 3CP without AsA. EPRI or OMRI imaging was started after addition of AsA/PBS solution (5 mM or 10 mM). Total volume of those phan-

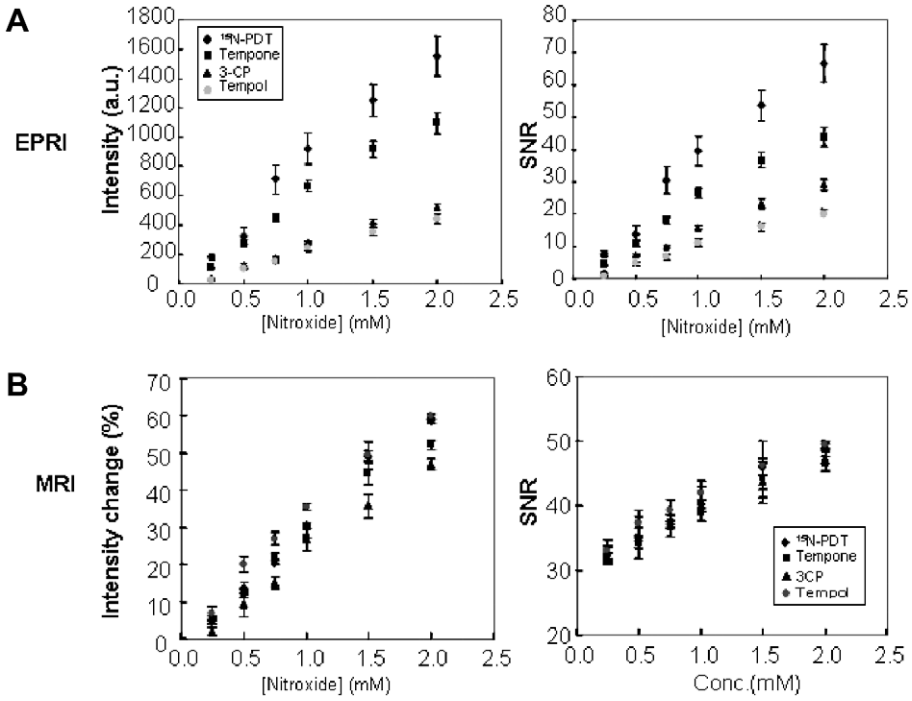

Fig. 3. Comparison of intensity change and SNR of nitroxides. The intensity change (left column) and SNR (right column) of nitroxides in (A) EPR and (B) MR images showed. The intensity was calculated for a select ROI from EPR and MR image of each nitroxides. The intensity change (%) of MRI was calculated based on the intensity of center phantom containing pure water. Number of experiments are 3.

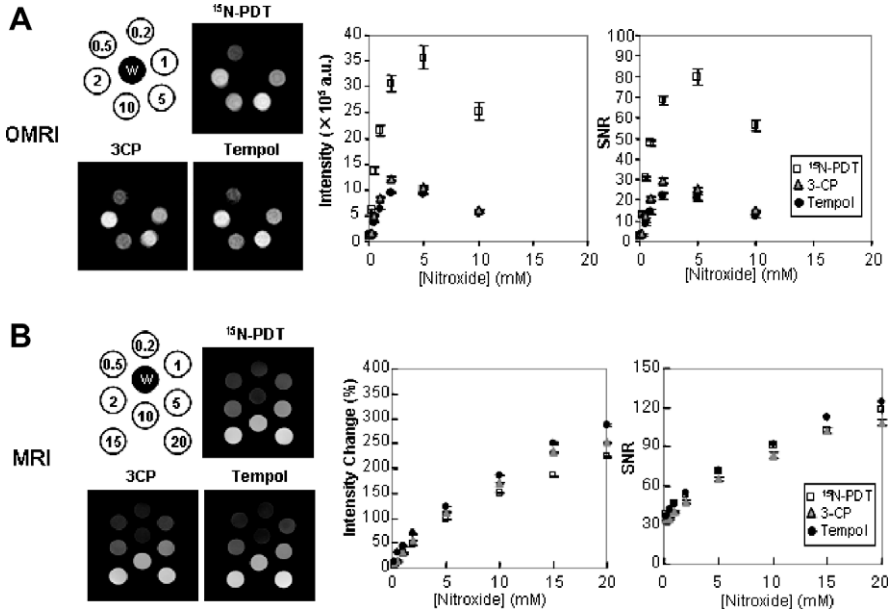

Fig. 4. Phantom images of OMRI and MRI using wide range of nitroxide concentrations. Schematics of the 3CP, Tempol and ^{15}N-PDT phantoms and (A) OMRI and (B) MRI images (left column). The phantoms contained 0.2–10 mM nitroxides for OMRI and 0.2–20 mM nitroxides for MRI, the signal intensity change (center column) and SNR (right column) are shown.

toms was 500 μL. In the case of MRI experiment, since it takes time to start the measurement after preparation of sample because of shimming and tuning, 2.5 mM 3CP phantoms were initially set in the magnet before addition of AsA solution. Then 100 μL of 25 and 50 mM AsA/PBS solution was added (final AsA concentrations 5 and 10 mM) to 2.5 mM 3CP solution phantoms (400 μL, final concentration is 2 mM) through the PE-10 tube (OD = 0.63 mm) 2 min after the imaging protocol was started. The experiments were repeated three or four times. Semi-logarithmic plots of the time course of image intensity change in the region of interest (ROI) were used to com-

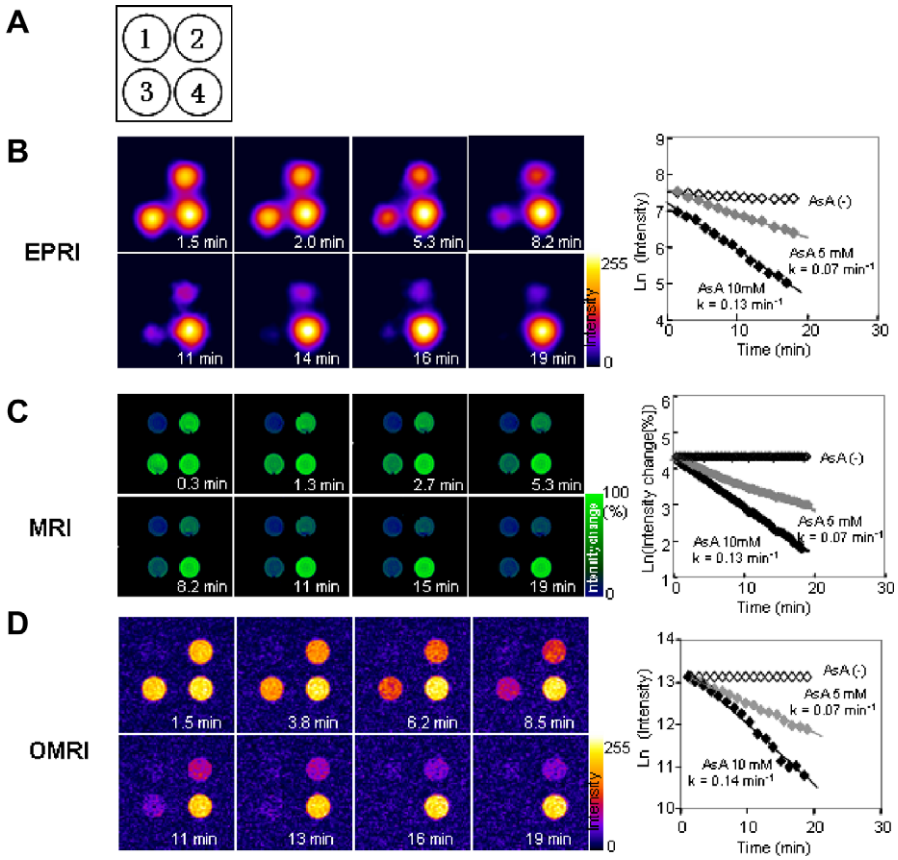

Fig. 5. Comparison of image intensity decay among three modalities. (A) Schematic of the phantoms: Tube 1, PBS; Tube 2, 2 mM 3CP and 5 mM AsA; Tube 3, 2 mM 3CP and 10 mM AsA; Tube 4, 2 mM 3CP. Time course images and decay slops of (B) EPRI, (C) MRI, (D) OMRI were obtained. After addition of AsA/PBS solution, the EPRI or OMRI measurements were started immediately and continuously measured up to 20 min. In the case of MRI, AsA/PBS was added using PE-10 tube 2 min after scanning was started. Therefore, time zero in the MRI experiment represents the time at addition of AsA solution. The experiments were repeated three or four times using with freshly prepared solutions. Semi-logarithmic plots of the time course of MRI signal change in the region of interest (ROI: 10×10 pixels) were used for decay rate calculation using imageJ software. Decay rate constants were obtained from the slope of linear portion of the decay curves.

pute the decay rates. The imaging conditions of EPRI, OMRI, and MRI experiments were follows; *EPRI*: RF, 300 MHz; radio frequency power, 2.5 mW; field modulation frequency, 13.5 kHz; field modulation amplitude, 0.8 G; time constant, 0.01 s; sweep width, 10 G; field gradient, 2.5 G/cm and number of averages, 2; approximate slice thickness, 25 mm (coil length) EPR image was reconstructed as a 128×128 matrix (FOV, 4.0 cm $\times$ 4.0 cm) by filtered back-projection method using Shepp-Logan filter. *OMRI*: TR, 1200 ms; TE, 25 ms; TEPR, 600 ms; number of phase-encoding gradient steps, 64; NEX, 1; FOV, 3.2 cm $\times$ 3.2 cm; slice thickness, 20 mm. *MRI*: TR, 75 ms; TE, 3 ms; Flip angle, 45°; NEX, 2; scan time, 20 s, image dimension, 256×256; FOV, 3.2 cm $\times$ 3.2 cm; slice thickness, 2.0 mm and number of slices, 2.

2.6. Image processing

The EPRI, MRI and OMRI data were analyzed using the ImageJ software package (http://rsb.info.nih.gov/ij/). T_1 maps were calculated to determine relaxation times in each tube of the phantom using a plug-in (MRI analysis calculator, Karl Schmidt, HypX Laboratory, Brigham and Women's Hospital) available in ImageJ. To obtain the relaxivity (it is the slope of relaxation rates as a function of concentration) the slope was calculated by the least squares method using relaxation rates ($1/T_1$). To measure signal to noise ratio (SNR), 6 points of ROI in noise area were randomly measured and averaged. The signal intensity of phantom was then divided by averaged noise intensity.

2.7. Results

The x-band EPR spectrum of ^{15}N-PDT under aerobic conditions at room temperature had the narrowest line width (0.26 ± 0.001G) followed by Tempone and 3CP were 0.40 ± 0.001 G and 1.08 ± 0.001 G, respectively. Tempol had lowest signal height in these nitroxides because of its relatively larger line width (1.50 ± 0.004 G).

Fig. 2 presents the EPR and MR images of a phantom object containing several different concentrations of nitroxides. Among the EPR images, the phantom containing 2 mM ^{15}N-PDT showed highest intensity compared with other nitroxides. Even the tube containing the lowest concentration (0.25 mM) can be readily identified in the phan-

tom. In the case of Tempol, adjacent tubes in the phantom were not well separated because of poor image resolution (Fig. 2E). On the other hand, the MR images showed similar intensity and resolution in all nitroxides (Fig. 2, right column). The differential change in relaxation induced intensity increase as a function of nitroxide concentration could not be easily discerned by simple inspection.

The change of EPR image intensity was linear as a function of the nitroxide concentrations ($R^2 = 0.99$ for all nitroxides). The intensities and slopes, which are related in dynamic range, were different depending on the individual nitroxides. If dynamic range is large, it shows better sensitivity in EPR detection. The slope was highest for the ^{15}N-PDT among the nitroxides tested (Fig. 3A). Additionally, for concentration >2 mM, the EPRI data exhibited deviation from the linear dependence (data not shown). In contrast, T_1 weighted image of water protons showed similar slopes and intensity change (%) in all nitroxides (Fig. 3B). The linear dependence of MRI intensity on nitroxide concentration persisted up to 5 mM ($R^2 = 0.98$) (Figs. 3 and 4B). Proton T_1 relaxivities of all nitroxides were not significantly different (0.16–0.18 mM^{-1} s^{-1}). For a meaningful quantitative comparison, the SNR of the images was computed and plotted in the right column of Fig. 3 (right column). The range of SNR of ^{15}N-PDT in EPRI was from 8 to 67. In contrast, all nitroxides showed similar SNR change from 32 to 49 in MRI. The SNR of water phantom in MRI was 34. Dynamic range of SNR in MRI was smaller compared to EPRI. It is to be noted, however, that EPRI intensity is the projection of the entire concentration of the solution in the tube corresponding to a pseudo-slice of 25 mm (the height of the solution in the tubes). On the other hand, the MRI intensity was originating from only a 2 mm thickness.

For the evaluation of OMRI, a seven tube phantom was imaged and compared with MRI (Fig. 4). The imaging experiments were extended up to 10 mM in nitroxide concentrations for OMRI and 20 mM for MRI experiments. The performance of OMRI was similar to that of EPRI, in terms of linewidth dependent sensitivity and non-linear concentration dependence above 2 mM (3CP and Tempol) or 5 mM (^{15}N-PDT) solution. Interestingly, MRI image intensity progressively increased even up to 20 mM in nitroxide concentration.

To assess the capabilities to monitor redox reactions, the three modalities were evaluated using the redox phantom comprising of 3CP and AsA (Fig. 5). All modalities tested were capable of monitoring the redox transformation in the 3CP phantom through its reaction with AsA. After mixing of AsA solution, image intensity gradually decreased, and decay rate of intensity was dependent on AsA concentration (Fig. 5 and Table 1). Approximately 19 min after the addition of AsA, image intensity in tube 3 completely disappeared in EPR and OMRI images, although MRI showed original proton images. Reduction rates were same among all these modalities, suggesting that any one of the methodology can evaluate the redox status (Table 1). However, the spatial and temporal resolution available from MRI was superior compared to EPRI or OMRI.

Table 1
Image parameters and comparison of three modalities of redox phantom experiments

	EPRI	OMRI	MRI
Field of view (mm)	40×40	32×32	32×32
Image resolution (mm)	>1	0.5	0.125
Slice thickness (mm)	25	20	2
Average	2	1	2
Slice	—	1	3 (max 6)
Scan time (s)	54	60	20
	$N = 3$	$N = 4$	$N = 3$
Decay rates (min^{-1})			
5 mM AsA	0.07 ± 0.004	0.07 ± 0.01	0.07 ± 0.01
10 mM AsA	0.14 ± 0.01	0.14 ± 0.002	0.13 ± 0.01

No significant difference among the modalities was observed in the *t*-test.

3. Discussion

With the availability of exogenous, non-toxic, bio-compatible free radical nitroxide probes, EPRI has shown its potential to provide, in a non-invasive manner, valuable information pertaining to redox status [3,4,28,29]. Metabolically responsive nitroxides are useful to non-invasively delineate tissue heterogeneity differences that may exist between normal and malignant tissue with respect to redox status, using EPRI, OMRI and high-field MRI. The present study was designed to evaluate each of these modalities for their potential in redox imaging.

EPR spectral intensities were dependent on spin of nitrogen nucleus (hyperfine splitting) and line width under the conditions of identical concentration and temperature. As expected, the image of ^{15}N-PDT, which exhibits a narrow doublet hyperfine pattern from the ^{15}N nucleus, showed the highest intensity and superior quality image (in terms of intensity and resolution) among nitroxides tested in this paper. On the other hand, image from the Tempol phantom could not be clearly visualized by EPRI because of the relatively large line width. Deconvolution procedure can eliminate the influence of the EPR line shape giving pure spatial information [30,31]. However, image intensity should be carefully re-normalized using signal intensities of zero gradient spectra obtained at suitable time points since the deconvolution process normalizes signal intensity. We have, however, not used any deconvolution procedures, and the images given are obtained by simple 2D filtered back-projection with a Shepp-Logan filter. In SPGR based T_1-weighted MRI, the resolution is not affected by EPR line width of nitroxide. Therefore, the MR images of the four nitroxides showed similar resolution and intensity change. The image enhancement in MRI is dependent on the original T_1 relaxation time and its variation by free radicals, which is related to the accessibility of the radical to water protons. In this paper, all nitroxides tested showed similar relaxivity. Image enhance-

ment in these nitroxides should be equal in tissue having the same T_1 relaxation time. On the other hand, image enhancement is affected by change of spectral shape and height in EPRI and OMRI. The near-independence of the proton relaxivity on the nature of nitroxide makes it easy to compare pharmacokinetics and redox status by MRI, whereas in OMRI and EPRI, the line width and spectral multiplicity determines the image quality in terms of resolution and dynamic range.

OMRI showed well resolved nitroxide images. The image intensity was dramatically affected by line width of the compound and experienced deep reduction in enhancement beyond 2 mM (3-CP and Tempol) or 5 mM (^{15}N-PDT), although image intensity went up in EPRI (albeit non-linear) and MRI, suggesting that OMRI enhancement is more sensitive to line broadening compared to EPRI. This is because the Overhauser enhancement is related to saturation of the EPR line which in turn depends on the line width. In contrast, the MR image intensity change was nearly linear up to 5 mM suggesting that we can use a much larger (nearly 2.5 times) nitroxide dose in MRI to improve the SNR, compared to EPRI or OMRI.

To evaluate the relative capabilities of EPRI, MRI, and OMRI using nitroxides as metabolically responsive probes, redox reactions driven by AsA to reduce the nitroxide 3CP to a diamagnetic state, was employed in all modalities. Continuous measurements of nitroxide levels examined detect similar decay rates from all three modalities (Fig. 5). The similar decay rates obtained from the phantom using MRI and EPRI, which is an accepted method in monitoring nitroxide levels validate the use of MRI for such studies. With MRI, multi-slice images were obtained in 20 s using SPGR method. This scanning allows fast pharmacokinetic imaging, besides providing detailed anatomical structure unlike in EPRI. In addition to anatomical structure, dynamic information such as blood flow, blood volume and water diffusion coefficients, etc., can be monitored by MRI and compared with redox images. Therefore, *in vivo* redox MR imaging using nitroxide can be a useful technique to monitor pharmacokinetics of nitroxide radicals. In particular, nitroxide such as Tempol, which has large line width and undergoes rapid in vivo reduction, will be a useful redox status-sensitive contrast agent. In this context, it is to be noted that the application of Tempol as a radioprotector to prevent alopecia is under phase I study [32].

4. Conclusion

EPRI and OMRI have several advantages to monitor nitroxide redox status. Dynamic ranges of image intensity in EPRI and OMRI are large compared to MRI, and spectral information leading to quantification of in vivo pO_2 is an additional bonus. However, the image quality and intensity are not as good as that of proton images in MRI. On the other hand, MRI can equally effectively provide in redox status and pharmacokinetics using nitroxides with the additional advantages of well resolved anatomical images and other functional information such as blood-volume, blood flow, water diffusion coefficient, etc.

References

[1] F.Q. Schafer, G.R. Buettner, Redox environment of the cell as viewed through the redox state of the glutathione disulfide/glutathione couple, Free Radic. Biol. Med. 30 (2001) 1191–1212.
[2] P. Kuppusamy, M. Afeworki, R.A. Shankar, D. Coffin, M.C. Krishna, S.M. Hahn, J.B. Mitchell, J.L. Zweier, In vivo electron paramagnetic resonance imaging of tumor heterogeneity and oxygenation in a murine model, Cancer Res. 58 (1998) 1562–1568.
[3] P. Kuppusamy, H. Li, G. Ilangovan, A.J. Cardounel, J.L. Zweier, K. Yamada, M.C. Krishna, J.B. Mitchell, Noninvasive imaging of tumor redox status and its modification by tissue glutathione levels, Cancer Res. 62 (2002) 307–312.
[4] K. Matsumoto, F. Hyodo, A. Matsumoto, A.P. Koretsky, A.L. Sowers, J.B. Mitchell, M.C. Krishna, High-resolution mapping of tumor redox status by magnetic resonance imaging using nitroxides as redox-sensitive contrast agents, Clin. Cancer Res. 12 (2006) 2455–2462.
[5] M.C. Krishna, A. Russo, J.B. Mitchell, S. Goldstein, H. Dafni, A. Samuni, Do nitroxide antioxidants act as scavengers of O^{2-} or as SOD mimics? J. Biol. Chem. 271 (1996) 26026–26031.
[6] M.C. Krishna, A. Samuni, J. Taira, S. Goldstein, J.B. Mitchell, A. Russo, Stimulation by nitroxides of catalase-like activity of hemeproteins. Kinetics and mechanism, J. Biol. Chem. 271 (1996) 26018–26025.
[7] M.C. Krishna, D.A. Grahame, A. Samuni, J.B. Mitchell, A. Russo, Oxoammonium cation intermediate in the nitroxide-catalyzed dismutation of superoxide, Proc. Natl. Acad. Sci. USA 89 (1992) 5537–5541.
[8] B.P. Soule, F. Hyodo, K. Matsumoto, N.L. Simone, J.A. Cook, M.C. Krishna, J.B. Mitchell, The chemistry and biology of nitroxide compounds, Free Radic. Biol. Med. 42 (2007) 1632–1650.
[9] H.M. Swartz, M. Sentjurc, P.D. Morse 2nd, Cellular metabolism of water-soluble nitroxides: effect on rate of reduction of cell/nitroxide ratio, oxygen concentrations and permeability of nitroxides, Biochim. Biophys. Acta 888 (1986) 82–90.
[10] J.L. Berliner, H. Fujii, Magnetic resonance imaging of biological specimens by electron paramagnetic resonance of nitroxide spin labels, Science 227 (1985) 517–519.
[11] L.J. Berliner, H. Fujii, X.M. Wan, S.J. Lukiewicz, Feasibility study of imaging a living murine tumor by electron paramagnetic resonance, Magn. Reson. Med. 4 (1987) 380–384.
[12] G. He, Y. Deng, H. Li, P. Kuppusamy, J.L. Zweier, EPR/NMR co-imaging for anatomic registration of free-radical images, Magn. Reson. Med. 47 (2002) 571–578.
[13] F. Hyodo, K. Yasukawa, K. Yamada, H. Utsumi, Spatially resolved time-course studies of free radical reactions through EPRI/MRI fusion technique, Magn. Reson. Med. 56 (2006) 938–943.
[14] T. Guiberteau, D. Grucker, Dynamic nuclear polarization imaging in very low magnetic fields as a noninvasive technique for oximetry, J. Magn. Reson. 124 (1997) 263–266.
[15] T. Liebgott, H. Li, Y. Deng, J.L. Zweier, Proton electron double resonance imaging (PEDRI) of the isolated beating rat heart, Magn. Reson. Med. 50 (2003) 391–399.
[16] D.J. Lurie, G.R. Davies, M.A. Foster, J.M. Hutchison, Field-cycled PEDRI imaging of free radicals with detection at 450 mT, Magn. Reson. Imag. 23 (2005) 175–181.
[17] M.C. Krishna, S. English, K. Yamada, J. Yoo, R. Murugesan, N. Devasahayam, J.A. Cook, K. Golman, J.H. Ardenkjaer-Larsen, S. Subramanian, J.B. Mitchell, Overhauser enhanced magnetic resonance imaging for tumor oximetry: coregistration of tumor anatomy and tissue oxygen concentration, Proc. Natl. Acad. Sci. USA 99 (2002) 2216–2221.
[18] H.J. Halpern, C. Yu, M. Peric, E. Barth, D.J. Grdina, B.A. Teicher, Oxymetry deep in tissues with low-frequency electron

paramagnetic resonance, Proc. Natl. Acad. Sci. USA 91 (1994) 13047–13051.
[19] H. Utsumi, K. Yamada, K. Ichikawa, K. Sakai, Y. Kinoshita, S. Matsumoto, M. Nagai, Simultaneous molecular imaging of redox reactions monitored by Overhauser-enhanced MRI with 14N- and 15N-labeled nitroxyl radicals, Proc. Natl. Acad. Sci. USA 103 (2006) 1463–1468.
[20] R.C. Brasch, D.A. London, G.E. Wesbey, T.N. Tozer, D.E. Nitecki, R.D. Williams, J. Doemeny, L.D. Tuck, D.P. Lallemand, Work in progress: nuclear magnetic resonance study of a paramagnetic nitroxide contrast agent for enhancement of renal structures in experimental animals, Radiology 147 (1983) 773–779.
[21] R.L. Ehman, G.E. Wesbey, K.L. Moon, R.D. Williams, M.T. McNamara, W.R. Couet, T.N. Tozer, R.C. Brasch, Enhanced MRI of tumors utilizing a new nitroxyl spin label contrast agent, Magn. Reson. Imag. 3 (1985) 89–97.
[22] H.M. Swartz, K. Chen, M. Pals, M. Sentjurc, P.D. Morse 2nd, Hypoxia-sensitive NMR contrast agents, Magn. Reson. Med. 3 (1986) 169–174.
[23] B. Gallez, G. Bacic, F. Goda, J. Jiang, J.A. O'Hara, J.F. Dunn, H.M. Swartz, Use of nitroxides for assessing perfusion, oxygenation, and viability of tissues: in vivo EPR and MRI studies, Magn. Reson. Med. 35 (1996) 97–106.
[24] C. Hayes, A.R. Padhani, M.O. Leach, Assessing changes in tumour vascular function using dynamic contrast-enhanced magnetic resonance imaging, NMR Biomed. 15 (2002) 154–163.
[25] A.R. Padhani, Dynamic contrast-enhanced MRI in clinical oncology: current status and future directions, J. Magn. Reson. Imag. 16 (2002) 407–422.
[26] F. Hyodo, K. Matsumoto, A. Matsumoto, J.B. Mitchell, M.C. Krishna, Probing the intracellular redox status of tumors with magnetic resonance imaging and redox-sensitive contrast agents, Cancer Res. 66 (2006) 9921–9928.
[27] J. Koscielniak, N. Devasahayam, M. Moni, P. Kuppusamy, K. Yamada, J.B. Mitchell, 300 MHz continuous wave electron paramagnetic resonance spectrometer for small animal in vivo imaging, Rev. Sci. Instrum. 71 (2000) 4273–4281.
[28] M. Elas, B.B. Williams, A. Parasca, C. Mailer, C.A. Pelizzari, M.A. Lewis, J.N. River, G.S. Karczmar, E.D. Barth, H.J. Halpern, Quantitative tumor oxymetric images from 4D electron paramagnetic resonance imaging (EPRI): methodology and comparison with blood oxygen level-dependent (BOLD) MRI, Magn. Reson. Med. 49 (2003) 682–691.
[29] K. Matsumoto, S. Subramanian, N. Devasahayam, T. Aravalluvan, R. Murugesan, J.A. Cook, J.B. Mitchell, M.C. Krishna, Electron paramagnetic resonance imaging of tumor hypoxia: enhanced spatial and temporal resolution for in vivo pO_2 determination, Magn. Reson. Med. 55 (2006) 1157–1163.
[30] K. Ohno, ESR imaging: a deconvolution method for hyperfine patterns, J. Magn. Reson. 50 (1982) 145–150.
[31] P. Kuppusamy, M. Chzhan, J.L. Zweier, Development and optimization of three-dimensional spatial EPR imaging for biological organs and tissues, J. Magn. Reson. B 106 (1995) 122–130.
[32] J.M. Metz, D. Smith, R. Mick, R. Lustig, J. Mitchell, M. Cherakuri, E. Glatstein, S.M. Hahn, A phase I study of topical Tempol for the prevention of alopecia induced by whole brain radiotherapy, Clin. Cancer Res. 10 (2004) 6411–6417.